ELSEVIER

Contents lists available at ScienceDirect

Earth and Planetary Science Letters

www.elsevier.com/locate/epsl



The many double BSRs across the northern Hikurangi margin and their implications for subduction processes



Shuoshuo Han ^{a,*}, Nathan L. Bangs ^a, Matthew J. Hornbach ^b, Ingo A. Pecher ^c, Harold J. Tobin ^d, Eli A. Silver ^e

- ^a Institute for Geophysics, The University of Texas at Austin, Austin, TX, 78758, USA
- ^b Southern Methodist University, Dallas, TX, 75205, USA
- ^c University of Auckland, Auckland, 1010, New Zealand
- ^d University of Washington, Seattle, WA, 98115, USA
- ^e University of California at Santa Cruz, Santa Cruz, CA, 95064, USA

ARTICLE INFO

Article history: Received 29 May 2020 Received in revised form 16 December 2020 Accepted 2 January 2021 Available online 15 January 2021 Editor: J.P. Avouac

Keywords: double bottom-simulating reflections (BSR) gas hydrate Hikurangi subduction zone rapid sedimentation tectonic uplift fluid migration

ABSTRACT

The bottom simulating reflection (BSR) is widely observed along continental margins and is believed to mark the base of gas hydrate stability zone (BGHSZ). In some regions, double or multiple overlapping BSRs are observed, yet their formation mechanisms and geologic implications are not well understood. Here we present 3D seismic images from the 2018 NZ3D experiment that covers a $14 \times 60~\text{km}^2$ survey area on New Zealand's northern Hikurangi subduction margin. We observe double BSRs in five locations. Beneath the Tuaheni Basin in the mid-slope, a secondary BSR (BSR2) lies $\sim 100\text{-}360~\text{m}$ deeper than the primary BSR (BSR1) and its 3D geometry mimics the unconformity at the base of the basin. At three thrust ridges located 18-38 km from the deformation front, BSR2 lies $\sim 55\text{-}130~\text{m}$ below and is subparallel to BSR1. At another thrust ridge $\sim 14~\text{km}$ from the deformation front, BSR2 forms above the BSR1, and the two BSRs converge towards the peak of the ridge. Through 3D modeling of BGHSZ and analysis of the geometry and reflection characteristics of the double BSRs, we identify three potential mechanisms for their formation (1) rapid sedimentation, (2) tectonic uplift, (3) overpressure/heat advection caused by fluid migration. Our study demonstrates that formation of double BSRs is closely linked to subduction processes along the northern Hikurangi margin, and double BSRs may be used as indicators for areas with recent sedimentation, tectonic and/or fluid activities.

© 2021 Elsevier B.V. All rights reserved.

1. Introduction

A bottom simulating reflection (BSR) is a seismic reflection that mimics the seafloor and crosscuts sediment layers. It is widely observed in the upper few hundred meters of marine sediments at continental margins, and is often associated with the presence of gas hydrate, an ice-like structure where methane or other gases are trapped in a cage formed by water molecules (Bohrmann and Torres, 2006). Gas hydrate is stable in high pressure and low temperature environments. At the base of the gas hydrate stability zone (BGHSZ), hydrate-bearing or water-bearing sediments lie above low-velocity gas-charged sediments. This negative impedance contrast gives rise to the reversed polarity of BSRs with respect to the positive impedance seafloor reflection (Haacke et al., 2007; Holbrook et al., 1996).

* Corresponding author.

E-mail address: han@ig.utexas.edu (S. Han).

At some locations, two or more overlapping BSRs are observed, for example at the Nankai trough (Foucher et al., 2002), the Hydrate Ridge of the Cascadia margin (Bangs et al., 2005), and the Black Sea (Popescu et al., 2006; Zander et al., 2017). While the primary BSR is regionally continuous and is generally consistent with the BGHSZ inferred from current pressure and temperature (P-T) conditions, the secondary BSR is usually more spatially limited and weaker in amplitude, and is separated from the primary BSR by several tens of meters. Many secondary BSRs also have reversed polarity, similar to the primary BSR (Bangs et al., 2005). It is noteworthy that although BSRs are widespread along continental margins, double or multiple BSRs are relatively rare.

The formation mechanisms of double/multiple BSRs are not well understood. The depth at which BSRs occur is determined by pressure, temperature, salinity of pore water, and the composition of gas (Sloan and Koh, 2007). Proposed mechanisms for double BSRs formation can be grouped into two categories. The first category assumes that both BSRs are in equilibrium with current P-T conditions, and they are associated with hydrate formed

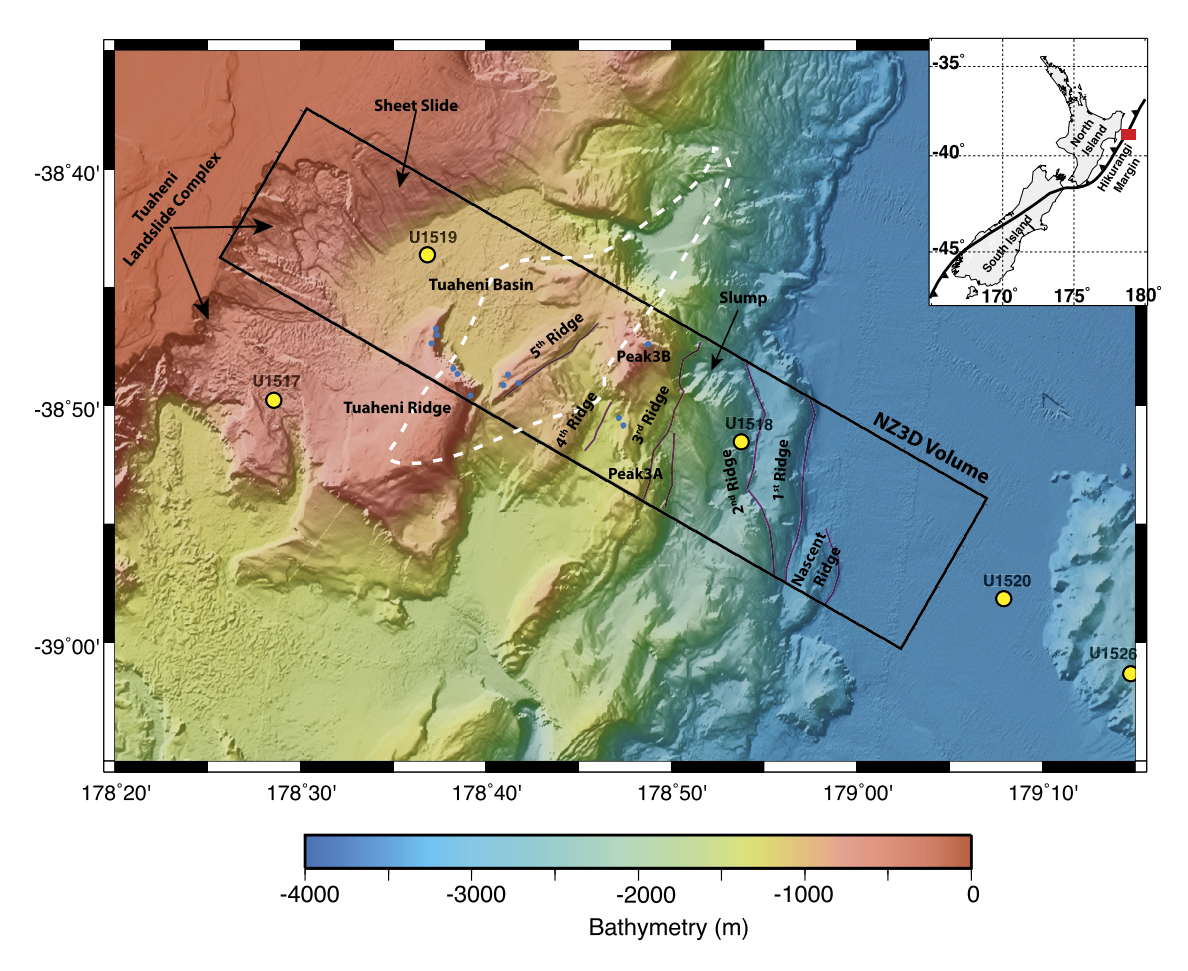


Fig. 1. Bathymetry map of study area on the northern Hikurangi subduction margin. Black rectangle: the extent of NZ3D seismic dataset. White dashed line: outline of a subducted seamount inferred from magnetic anomalies (Barker et al., 2018). Blue dots: seep sites inferred from acoustic anomalies in the water column data acquired during the NZ3D experiment. Purple lines: traces of major thrust faults at the seafloor. Yellow dots: IODP Exp. 372/375 drilling Sites U1517-U1526. Inset: regional tectonic setting. (For interpretation of the colors in the figure(s), the reader is referred to the web version of this article.)

from different gases (Andreassen et al., 2000). For example, while the shallow BSR marks the BGHSZ for methane hydrate (Structure-I gas hydrate), the deeper BSR occurs at the BGHSZ for hydrate formed by gas containing higher order hydrocarbons (Structure-II gas hydrate). Although Structure-II hydrate has been sampled in a few locations including Gulf of Mexico (Milkov and Sassen, 2000) and offshore Borneo (Paganoni et al., 2016), it has not been recovered at a location where double BSRs are observed. Thus this mechanism has not been confirmed. The second category assumes that one of the BSRs is in equilibrium with current or very recent P-T conditions, yet the other BSR is a relic BSR in the process of dissipating due to changing P-T conditions. Proposed mechanisms for changing P-T conditions include changes in bottom water temperature (BWT) and sea level due to climate changes (Bangs et al., 2005; Popescu et al., 2006), tectonic uplift and subsidence (Foucher et al., 2002; Pecher et al., 2017), and sedimentation and erosion (Crutchley et al., 2011; Zander et al., 2017). Yet due to large uncertainties in past climate conditions and tectonic history, these proposed mechanisms are in general not well constrained.

Along the Hikurangi subduction margin offshore New Zealand, double BSRs have been previously observed at two locations from 2D seismic lines. At Western and Eastern Porangahau Ridge along the southern Hikurangi margin, Crutchley et al. (2011) report closely spaced double BSRs (separation <50 ms two-way-traveltime) and suggest one of the BSRs may be a relic BSR formed prior to seafloor erosion or enhanced heat flow. In the northern Hikurangi margin, two BSRs separated by \sim 70-120 m are imaged near the pinch-out of the BGHSZ in the upper slope and are proposed

to form by tectonic uplift (Pecher et al., 2017). However due to the isolated observations, whether these double BSRs formed only from local processes, or are related to broader-scale tectonic processes is not clear.

In this study, we present 3D seismic images covering an area of $14 \times 60 \text{ km}^2$ from the 2018 NZ3D experiment along the northern Hikurangi margin (Fig. 1). We observe double BSRs at multiple locations beneath several thrust ridges and a mid-slope basin (Figs. 2-5). Through analyses of 3D geometry and reflection characteristics of the double BSRs, modeling of BGHSZ and paleo-seafloor, and incorporation of drilling data from International Ocean Discovery Program (IODP) Expeditions 372 & 375 (Pecher et al., 2019; Wallace et al., 2019), we investigate the origins of these double BSRs in relation to subduction processes. In particular, we identify three potential mechanisms for double BSRs formation associated with rapid sedimentation, tectonic uplift, overpressure/heat advection caused by fluid migration. Our new data provide better constraints and new insights into the formation processes of double BSRs. Our study also demonstrates that the dynamics of gas hydrate systems along the northern Hikurangi margin is closely linked to subduction processes, and double BSRs may be useful indicators for revealing areas with recent sedimentation, tectonic and/or fluid activities in subduction zone studies.

2. Tectonic setting

The Hikurangi trough lies offshore the east coast of New Zealand's North Island. Here the Pacific plate subducts west-

ward beneath the Australia plate at convergence rate of 45-55 mm/yr (Wallace et al., 2004). The subducting Hikurangi Plateau, a Mesozoic-age large igneous province with anomalously thick (\sim 10-15 km) crust (Davy et al., 2008), is studded by numerous seamounts (Pedley et al., 2010). The accretionary wedge at the northern Hikurangi margin is relatively small and is interpreted as resulting from repeated erosion by subducting seamounts (Collot et al., 2001; Pedley et al., 2010). Subducted seamounts beneath the wedge have also been inferred from seismic reflection profiles and modeling of magnetic data (Barker et al., 2018; Bell et al., 2014). The plate interface along the northern Hikurangi margin is characterized by shallow locking and aseismic creeping. Slow slip events (SSEs) are observed to occur here every 1-2 years at shallow depth (<15 km), with relatively short duration (<1 month) and a range of equivalent earthquake magnitudes from events of $M_w > 7.0$ to events of $M_w 6.0 \sim 6.5$ (Wallace, 2020).

3. Data and methods

In January and February of 2018 we acquired a 3D seismic data volume within a $14 \times 60 \text{ km}^2$ survey area aboard the R/V Langseth along the northern Hikurangi margin (Fig. 1). Two groups of airgun arrays, each includes 18 guns with a total volume of 3,300 in³ (54 L), were towed at a nominal depth of 7 m and fired alternately every 25 m. The data were recorded with four 6-km-long, solid-state streamers towed at a nominal depth of 8 m with 150 m spacing. Each streamer is composed of 468 active hydrophone groups spaced at 12.5 m. Positions of sources and receivers were derived from shipboard and tailbuoy GPS receivers, compass-enhanced DigiCourse birds and an acoustic transponder array placed along the streamers. Data were recorded in 9.5-s long records with a sampling rate of 2 ms.

The 3D processing sequence includes 3D geometry definition (bin size 25 m \times 37.5 m), filtering to remove cable noise, trace editing, spherical divergence correction, resampling to 4 ms, velocity analysis, stacking, and 3D Kirchhoff post-stack time migration using stacking velocity. A starting velocity model was built by expanding a 2D velocity profile going through the NZ3D area that was derived from traveltime tomography on 12.5 km offset streamer data to 3D (A. Arnulf, personal communication). Highresolution multi-beam bathymetry acquired during our survey was used to define the seafloor of the 3D velocity model. Semblancebased velocity analysis (Schneider and Backus, 1968) was then conducted on every 30 inlines (1.125 km) and 50 crosslines (1.25 km) to refine the velocity model (Fig. S1). The uncertainty of the velocity is estimated to be $\sim \pm 5\%$ within the depth ranges of the BSR for most places, but can be higher in areas with no clear reflections. Multiple suppression was not applied as our target depths are all above the water column multiple. Depth conversion was applied to the 3D migrated images using interval velocities derived from stacking velocity (Fig. S1). From the depth converted 3D volume, we interpreted BSRs, faults, unconformities, and other relevant horizons.

To investigate whether the gas hydrate system at this part of the northern Hikurangi margin is in thermodynamic equilibrium, we conducted 3D modeling of BGHSZ in steady state conditions following the approach of Hornbach et al. (2012) (Supplementary Information). We constructed a starting temperature field from XBT measurements of water column temperature during the NZ3D experiment (Fig. S2), bathymetry encompassing the survey area, and an initial thermal gradient. We ran the model over a simulated period of 1 Myr to allow the temperature field to reach the final steady state. BSR depth is calculated using a pure methane gas hydrate stability curve with pore water salinity of 3.45%, assuming hydrostatic pressure at the BSR depth (Sloan and Koh, 2007).

4. Results

4.1. Slope structure within NZ3D area

Our study area on the northern Hikurangi margin is characterized by a steep lower slope consisting of new thrust ridges, a mid-slope basin (the Tuaheni Basin) overlying older thrust ridges, and a gently dipping upper slope that has failed with submarine landslides (Fig. 1).

Within $\sim\!\!23$ km from the deformation front, the seafloor shallows from $\sim\!\!3500$ m to $\sim\!\!900$ m across five thrust ridges (Fig. 1). The orientation of the thrust ridges is approximately N-S near the deformation front, but changes to NE-SW at the 5th (the most landward) ridge. A major slump that is $\sim\!\!3.5$ km across with a scarp $\sim\!1.2$ km high is present at the northern end of the 2nd ridge. A few smaller scale slumps are also observed along the 1st, 2nd, and 3rd ridges (Fig. 1).

In the middle slope, the Tuaheni Basin lies between the 5th ridge and the upper slope and is bounded by the Tuaheni Ridge to the south (Fig. 1). The basin is \sim 19 km long (in the NE-SW direction) and 12 km wide. While the basin area is mostly flat, high-resolution bathymetry reveals fine-scale blocky appearance and streaks at the seafloor, which may indicate debris flow deposits (Fig. 1). The basin fill sediments are deposited on top of older thrust ridges and lap onto the upper slope (Fig. 3). The unconformity that marks the base of the basin shows the shape of a channel oriented NE-SW in the western part of the basin, subparallel to the 5th ridge and the seaward edge of the upper slope (Fig. 3a). This channel is shallow (\sim 130-140 mbsf) and narrow (\sim 1.2 km) in the SW and gradually widens (to \sim 2.4 km) and deepens (to \sim 600 mbsf) to the NE. The upper 150-160 m of the basin deposit is relatively chaotic whereas the deeper section consists of strongly reflective layers (Fig. 3b-d). Both the upper and the lower sections show slight tilt in the east, likely in response to the deformation of the underlying thrust ridges (Fig. 3b, d).

The upper slope is composed of a section of seaward dipping wedge deposits (Fig. 3b). Arcuate-shaped head scarps across the upper slope mark several episodes of slope failure in the southern part of our 3D survey area (Fig. 1). They are part of the Tuaheni Landslide Complex (Mountjoy et al., 2009). To the north, sheet slides have removed the topmost ~20-30 m of strata from the upper slope (Fig. 1).

4.2. Distribution and characteristics of double BSRs

Within the NZ3D volume, BSRs are observed from upper slope to near the deformation front (Fig. 2). The BSR appears as a reflection with negative polarity that follows the seafloor in most areas (e.g. Fig. 4). It is in general a regionally continuous reflection but is not imaged or difficult to identify beneath the main outlet of slope failures, the northwestern edge and eastern portion of the Tuaheni Basin, or around the slump areas (Fig. 2a). We interpret this BSR as the primary BSR and label it as BSR1.

At five locations within the NZ3D volume we also observe a second BSR in discrete patches with dimensions of a few kilometers below or above the more regionally continuous BSR1 (Fig. 2b). We consider these BSRs (labeled as BSR2) to be secondary BSRs because of their more limited spatial extent relative to BSR1. As for BSR1, BSR2 also crosscuts sediment strata (Figs. 3–5). In areas where the reflection is strong enough to discern its polarity, the BSR2 appears to be of negative polarity, similar to the BSR1 (Figs. 3e-g, 5c-f).

4.2.1. Tuaheni Basin

The largest BSR2 patch (Patch A) forms across the western part of the Tuaheni Basin (Figs. 2-3). This 5.5 km \times 2 km patch strikes

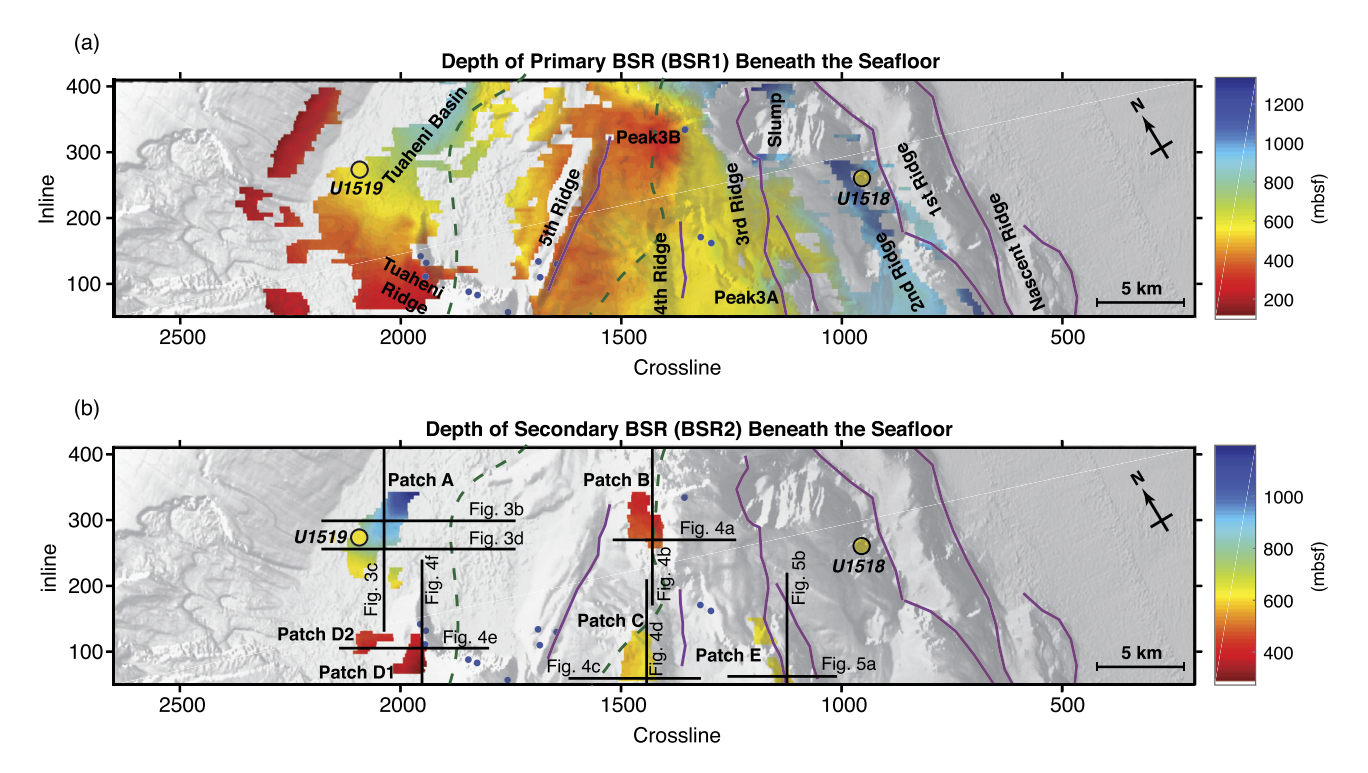


Fig. 2. Depth of primary BSRs (a) and secondary BSRs (b) beneath the seafloor. Green dashed line: outline of a subducted seamount inferred from magnetic anomalies (Barker et al., 2018). Blue dots: seep sites inferred from acoustic anomalies in the water column data acquired during the NZ3D experiment. Purple lines: traces of major thrust faults at the seafloor. Yellow dots: IODP Exp. 372/375 drilling Sites U1518 and U1519. Locations of the example inlines and crosslines in Figs. 3–5 are shown in (b).

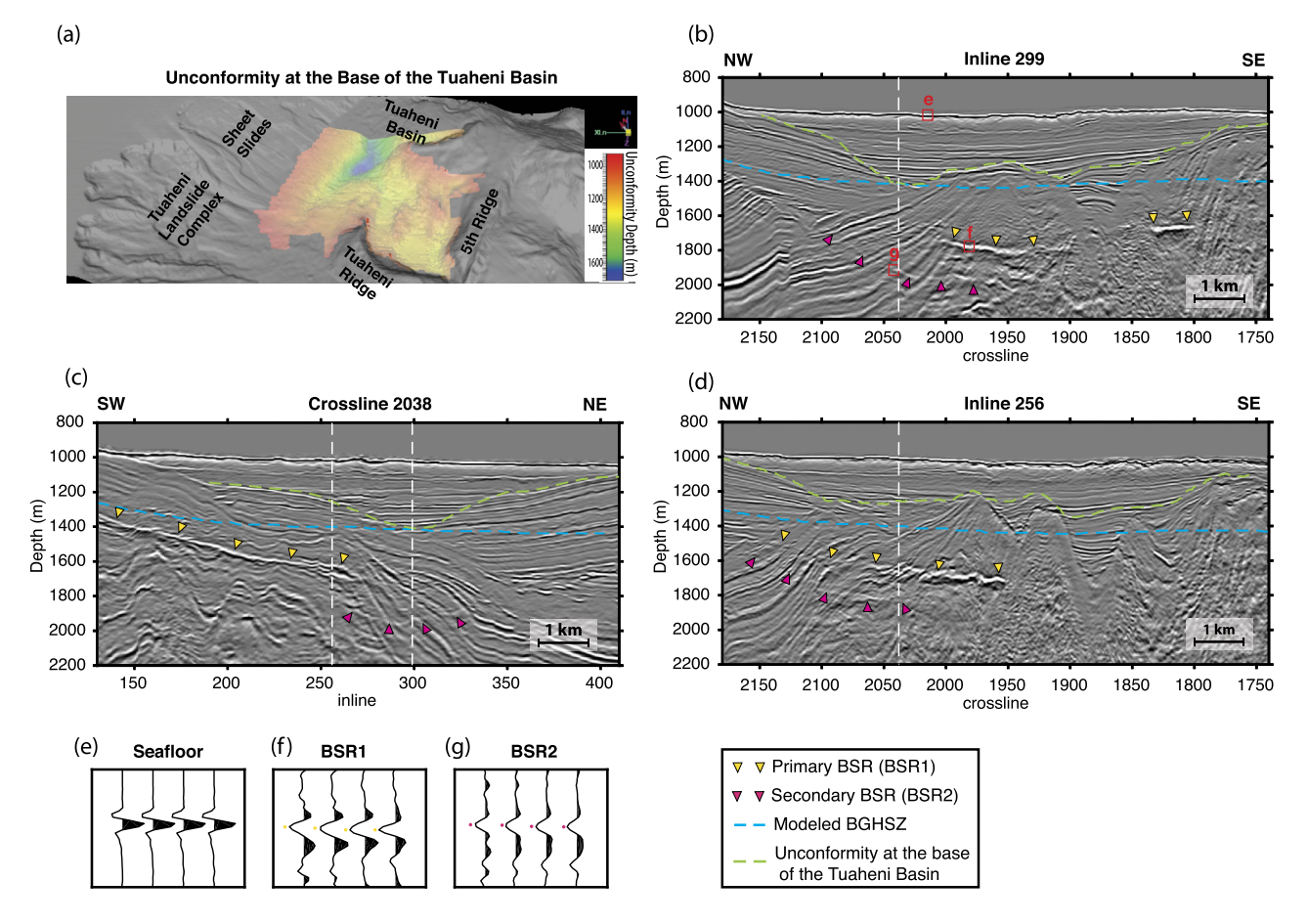


Fig. 3. Double BSRs beneath the Tuaheni Basin (Patch A). (a) Topography of the unconformity at the base of the Tuaheni Basin. (b-d) Seismic images of BSR1 and BSR2 along example inlines and crossline, superimposed by modeled steady state BGHSZ and interpreted unconformity at the base of the basin. Vertical white dashed lines indicate crossing line locations. Time sections of the seismic images are in Fig. S4. (e-g) Waveforms of the seafloor, BSR1, and BSR2 reflections with polarity indicated by colored dots.

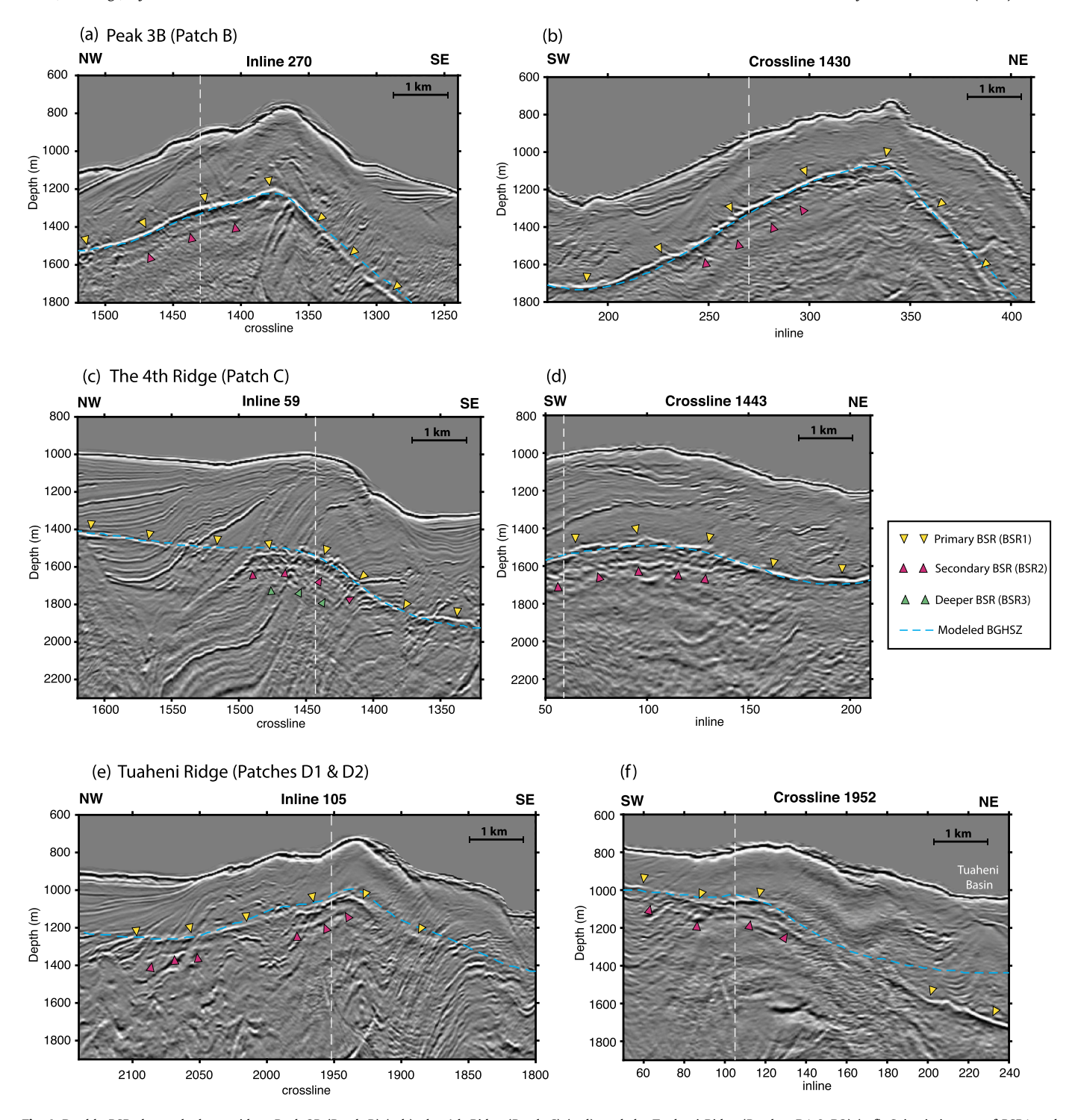


Fig. 4. Double BSRs beneath thrust ridges Peak 3B (Patch B) (a-b), the 4th Ridge (Patch C) (c-d), and the Tuaheni Ridge (Patches D1 & D2) (e-f). Seismic images of BSR1 and BSR2 along example inlines and crosslines are superimposed by modeled steady state BGHSZ. Vertical white dashed lines indicate crossing line locations. Time sections of the seismic images are in Fig. S5.

NE-SW, sub-parallel to the long axis of the basin (Fig. 2b). Here both BSR1 and BSR2 occur within the thrust ridges underlying the basin deposit, significantly deeper than the modeled steady-state BGHSZ at this location (Fig. 3b-d). BSR2 is a much weaker reflection than the BSR1 and crosscuts the dipping strata of the thrust ridges. There is no apparent change in reflection amplitude of these dipping strata across the BSR2. In places, BSR2 lies beneath the expected position of BSR1 but BSR1 is not seen (Fig. 3b-c). Similar to the BSR1, BSR2 does not mimic the flat seafloor, but instead it deepens from 600 to 1180 mbsf, toward the center of the basin

and towards the NE where the basin deposit thickens (Fig. 2). The separation between BSR1 and BSR2 also increases from $\sim\!100$ m in the SW to $\sim\!360$ m in the NE. The 3D shape of BSR2 Patch A resembles the unconformity that separates the basin fill deposit and the underlying thrust ridges (Figs. 2–3).

4.2.2. Thrust ridges

BSR2 is also present in patches beneath the flanks and/or peaks of four thrust ridges located 14 to 38 km landward of the defor-

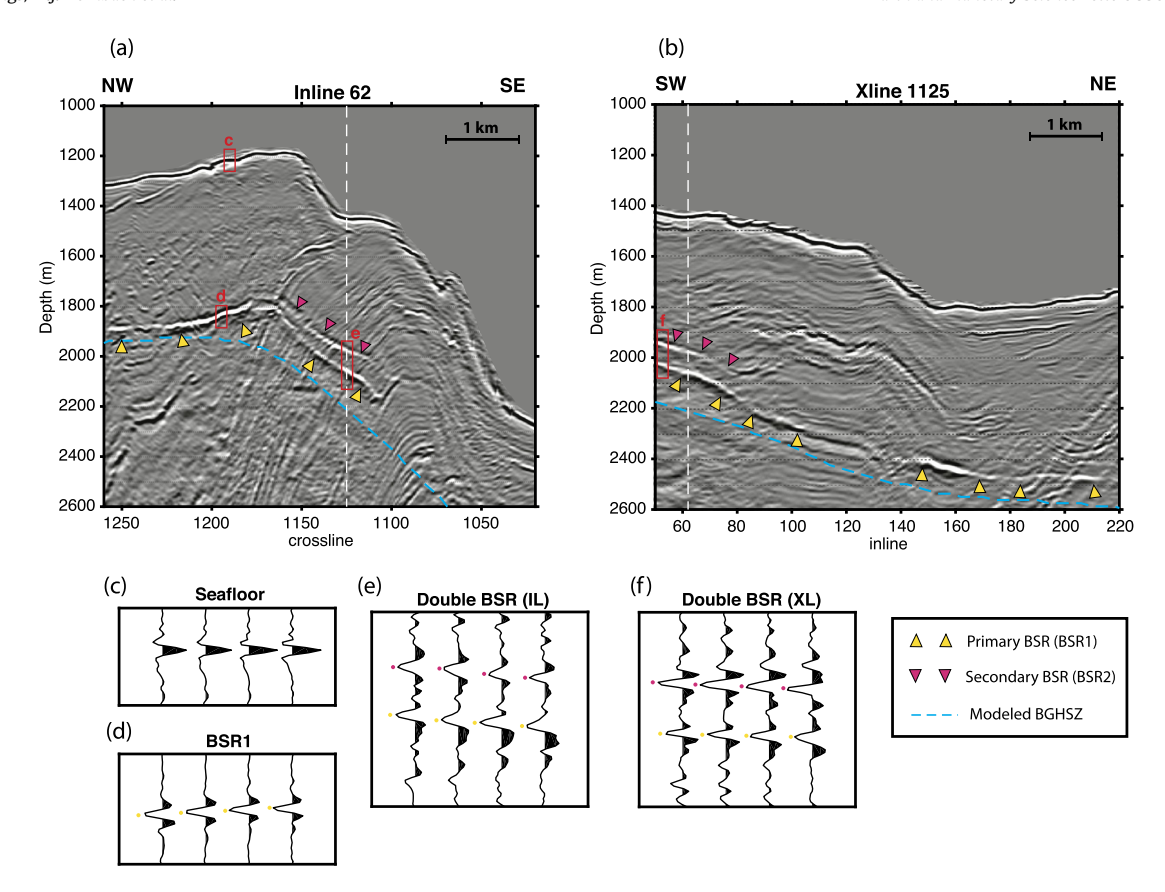


Fig. 5. Double BSRs beneath thrust ridge Peak 3A (Patch E). (a-b) Seismic images of BSR1 and BSR2 along example inline and crossline are superimposed by modeled steady state BGHSZ. Vertical white dashed lines indicate crossing line locations. Time sections of the seismic images are in Fig. S6. (c-f) Waveforms of the seafloor, BSR1, and BSR2 reflections with polarity indicated by colored dots.

mation front (Fig. 2b). These BSR2 patches are \sim 2-3 km across and lie \sim 55-130 m below or above BSR1 (Figs. 2b, 4, 5).

The double BSRs beneath Peak 3B (Patch B), the 4th Ridge (Patch C), and the Tuaheni Ridge (Patches D1 and D2) share a number of similarities (Fig. 4): (1) BSR2 lies below and is sub-parallel to BSR1; (2) BSR2 is in general a weaker reflection than BSR1; and (3) BSR1 fits the modeled steady-state BGHSZ well (except for one example shown in Fig. 4f, where the ridge is adjacent to the basin) and BSR2 is deeper than the modeled BGHSZ. These BSR2 patches also have some differences. While Patches B and D are located beneath the landward flank of the ridges, Patch C is located beneath the peak (Fig. 4a, c, e). Furthermore, there is another reflection, potentially a third BSR (labeled as BSR3), beneath the southern end of Patch C (Fig. 4c).

The double BSRs imaged beneath Peak 3A at the south side of the 3rd thrust ridge (labeled as Patch E) show several unique characteristics compared to double BSRs at other ridges (Fig. 5). The double BSRs occur beneath the seaward flank of the Peak 3A within a section of steeply dipping strata. Instead of being subparallel to each other, the two BSRs are separated by \sim 60-120 m at their seaward end and converge towards the ridge peak (Fig. 5a). Both BSRs are bright reflections. Although their waveforms are more complex than normal BSR1 reflection elsewhere, and show spatial variations, their polarity is in general negative (Fig. 5c-f). While it is not clear from inline images which BSR is primary and which is secondary, the crossline images show that the deeper BSR is more regionally continuous than the shallower one (Fig. 5b). Thus we regard the deeper BSR as BSR1 and the shallow one as BSR2. Both BSRs are significantly shallower than the modeled steady state BGHSZ beneath Peak 3A (inline 50-90, crossline 11001200); but outside of the double BSRs area, the BSR1 lies close to the modeled BGHSZ (Fig. 5).

5. Formation of double BSRs

The position of a BSR is closely related to P-T conditions and gas composition. The occurrence of double/multiple BSRs has been proposed to mark the BGHSZs for hydrates with different gas compositions (Andreassen et al., 2000). In our study area, ocean drilling by IODP Exp. 372&375 found that methane is dominant in gas composition (> 99.8%) and higher order hydrocarbon gases such as ethane and propane only exist in trace amounts, not enough to form Structure-II hydrate (Pecher et al., 2019; Wallace et al., 2019). Extensive sediment coring in the past decade also suggests purely biogenic methane generation in this part of the Hikurangi Margin (Crutchley et al., 2016; Greinert et al., 2010; Huhn, 2016). The penetration depths of most of these drill sites are within the stability zone of methane hydrate, so it is possible that more higher order hydrocarbon gases exist at greater depth due to compositional fractionation, but are not sampled (Paganoni et al., 2016). While fractionation of thermogenic gas has been suggested to cause double BSRs, we are not aware of any locations globally where this process has been confirmed. Therefore we consider it unlikely that the BSR2s in our 3D dataset are formed from Structure-II hydrate. We focus our discussion below on the more likely cause of BSR2 formation, which is change of BGHSZ for methane hydrates following changes in P-T conditions in this region.

The simplest cause of changes in P-T conditions at the GHSZ are changes in sea level and BWT due to glacial cycles, which have been proposed to explain the double BSRs formation in some regions (Bangs et al., 2005; Popescu et al., 2006). Rising sea

level during deglaciation is usually accompanied by BWT warming, while the opposite occurs during glaciation (Ruppel and Kessler, 2017; Screaton et al., 2019). Thus changes of sea level and BWT have opposing effects on BGHSZ depth. The BWT history in our study area is not well known. Recent modeling study shows that BWT changes of 2 °C during glacial cycles would mostly counteract the impacts of sea level change along the northern Hikurangi margin (Screaton et al., 2019). Furthermore, the dominant ocean current in this region is the East Cape Current that flows southwestward along the east coast of the North Island. Within our study area, there are no permanent eddies, nor is there major upwelling/downwelling (Chiswell et al., 2015). CTD measurements of water column temperature in our study area show minimal spatial variations (Fig. S2). Thus changes in sea level and BWT should have a regional effect, at least on the scale of our survey area, and BSR2 should mimic the seafloor and BSR1. Yet BSR2 in the Tuaheni Basin does not follow the seafloor bathymetry and BSR2 beneath the Peak 3A converges with the BSR1. Therefore changes in BWT and sea level are not sufficient or necessary to explain our observation of double BSRs from the NZ3D data.

In the following sections we analyze sedimentation, tectonic, and fluid processes related to subduction along the northern Hikurangi margin and assess their roles in changing the P-T conditions that facilitate double BSRs formation (Figs. 6–9).

5.1. Double BSRs beneath the Tuaheni Basin

The Tuaheni Basin lies at the base of the upper slope and has been filled in with periodic landslide deposits (Mountjoy et al., 2009). The rapidly deposited sediments depress the near surface thermal gradient and induce heat to flow upward. As the thermal gradient is restored, the BGHSZ migrates upward and a new BSR forms at shallower depth (Fig. 9a).

If rapid sedimentation has caused the BGHSZ to shift from BSR2 to a shallower depth, we expect BSR2 to be in a position in equilibrium with pre-deposition P-T conditions. We can therefore model the paleo-seafloor (paleoSF) when BSR2 formed from the observed BSR2 depth. This inverse approach does not require any a priori information about paleoSF. For simplification, we assume a uniform thermal gradient $(\frac{dT}{dz})$ beneath **paleoSF** and a uniform BWT at paleoSF ($T_{paleoSF}$). With hydrostatic pressure and a pure methane stability curve, we can obtain the temperature at BSR2 level (T_{BSR2}) when it is in equilibrium. We can then calculate the depth of paleoSF $Z_{paleoSF} = Z_{BSR2} - (T_{BSR2} - T_{paleoSF}) / \frac{dT}{dz}$. We tested different combinations of $\frac{dT}{dz}$ and $T_{paleoSF}$. Our results show that the modeled paleoSFs do not follow the current flat seafloor but plunge from SW to NE. The **paleoSF** modeled with $\frac{dT}{dz}$ of 24.3 °C/km and T_{paleoSF} of 4°C lies remarkably close to the unconformity between the basin deposit and the underlying old thrust ridges, mapped in three dimensions (Fig. 3a) – the ratio between $\boldsymbol{Z_{paleoSF}}$ and the depth of unconformity ($\textbf{Z}_{\textbf{unconformity}})$ is 1 ± 0.04 for most of the surface (Fig. 6). This close match of the two surfaces leads us to conclude that the BSR2 formed when this unconformity was the paleo-seafloor, before rapid filling of the basin. It is noteworthy that $\frac{dT}{dz}$ of 24.3 °C/km is the value obtained from APCT measurements at IODP Site U1519 (Pecher et al., 2019), suggesting that the background thermal gradient when BSR2 formed may be similar to the current value. We recognize that $\frac{dT}{dz}$ and $T_{paleoSF}$ may vary spatially and future models that take into account these spatial variations could further improve the geometry of the modeled paleo-seafloor.

If our inference that BSR2 existed before the deposition in the Tuaheni Basin is correct, the age of basin deposit can be used to constrain the age of the BSR2. IODP Site U1519 is located at the landward edge of the Tuaheni Basin (Fig. 1). Biostratigraphy at this

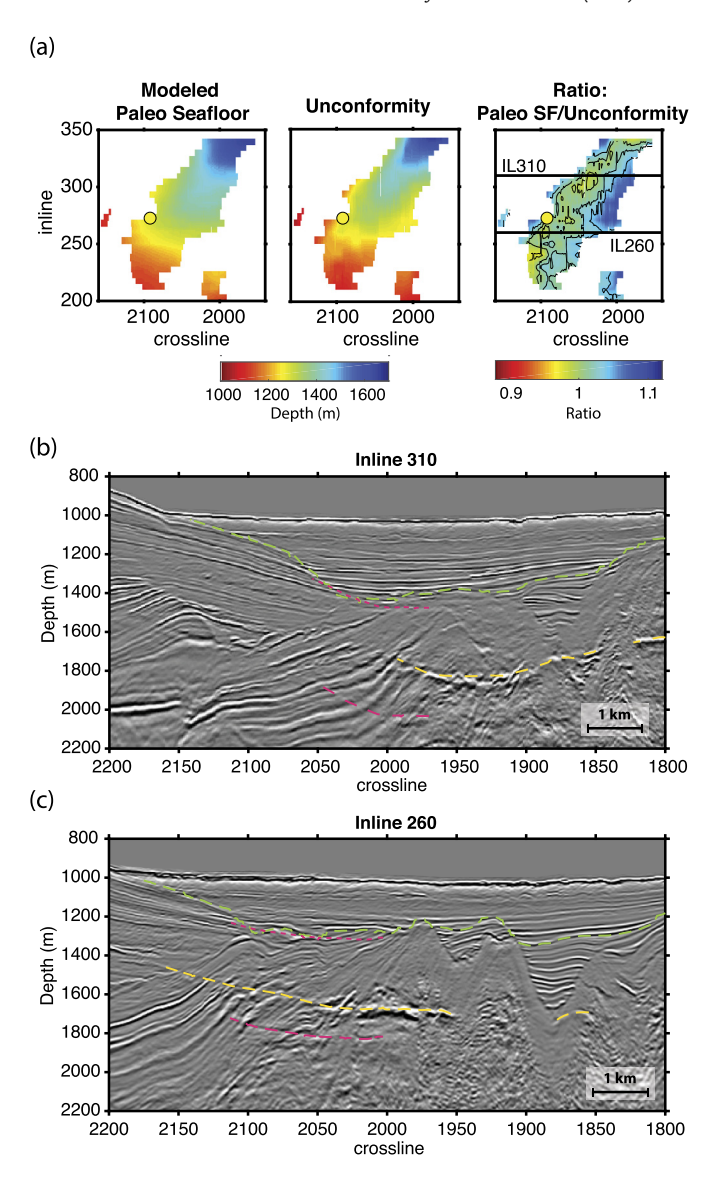


Fig. 6. Comparison of paleo-seafloor modeled from BSR2 and the unconformity at the base of the Tuaheni Basin. (a) Depths of paleo-seafloor modeled from BSR2, depth of the unconformity (cropped to the portion overlaps with the modeled paleo-seafloor), and their ratio, with contours at 0.96 to 1.04 at 0.02 intervals. (b-c) Example inlines showing comparison of the unconformity and the modeled paleo-seafloor. Yellow dashed line: interpreted BSR1; Magenta dashed line: interpreted BSR2; Magenta dotted line: paleo-seafloor modeled from BSR2; Green dashed line: interpreted unconformity at the base of the Tuaheni Basin.

site only provides crude age estimate due to large coring gaps. Beneath the top Holocene section (0–14 m), the section between 14 and 536 mbsf, which includes the basin-fill deposit, the seaward dipping upper slope deposit, and the uppermost part of the underlying thrust ridge, is dated Late to Middle Pleistocene (Wallace et al., 2019). More detailed age models are not available yet. Very weak reflections of BSR2 suggest that they are likely caused by small amount of residual gas beneath the paleo-BGHSZ. The low concentration of free gas inhibits it to form a buoyant phase and migrate upward, thus the gas can be trapped at the paleo-BGHSZ level for many kyrs, preserving the BSR2.

BSR1 beneath the Tuaheni Basin also deepens towards the NE, and does not follow the current flat seafloor (Figs. 2a, 3). As with BSR2, BSR1 is also significantly deeper than the modeled BGHSZ, which suggests that it is also out of equilibrium with current P-T conditions (Figs. 3, S3). The 3D shape of the BSR1 mimics the major unconformity in some parts of the basin (Fig. 3c), but not

Table 1Summary of abbreviations and symbols in Section 5.

paleoSF	Pre-deposition seafloor	Z _{BSR2}	Depth of BSR2	R_2	Slip rate along the splay fault
$\frac{dT}{dz}$	Thermal gradient	Zunconformity	Depth of unconformity at the base of the Tuaheni Basin	R_v	Uplift rate
T _{paleoSF}	Water bottom temperature at paleoSF	α	Dip of plate interface megathrust	Phydro	Hydrostatic pressure
T _{BSR2}	Temperature at BSR2 level	β	Dip of upper plate thrust fault	P _{litho}	Lithostatic pressure
$Z_{paleoSF}$	Depth of paleoSF	R_1	Full convergence rate along the plate interface	λ^*	Overpressure ratio

everywhere, suggesting that the BSR1 may have formed when the basin was partially filled (Fig. 9a). It is possible that the basin was filled by two episodes of rapid deposition and the BSR1 was in equilibrium with the seafloor after the 1st episode. After the basin was fully filled by a 2nd episode of deposition, the BSR1 has been in transient state moving upward to the current BGHSZ. The apparent depth discrepancy between BSR1 and the modeled BGHSZ is subject of an ongoing study.

5.2. Double BSRs beneath thrust ridges

Aside from the BSR2 patch beneath the Tuaheni Basin, all other BSR2 patches are located beneath thrust ridges. These thrust ridges are underlain by thrust faults that stem from the subduction megathrust. During subduction, convergence can be accommodated by slip along these upper plate thrust faults, which would uplift the ridges and reduce pressure of the water column. Thrust faults or highly dipping strata can also facilitate upward fluid migration from the megathrust to shallow sediments at thrust ridges, modulating the P-T conditions there. Here we consider the effects of these subduction-related processes on the formation of double BSRs at the thrust ridges.

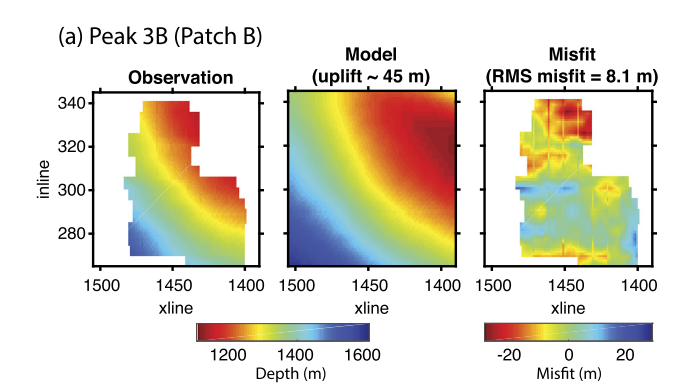
5.2.1. Tectonic uplift

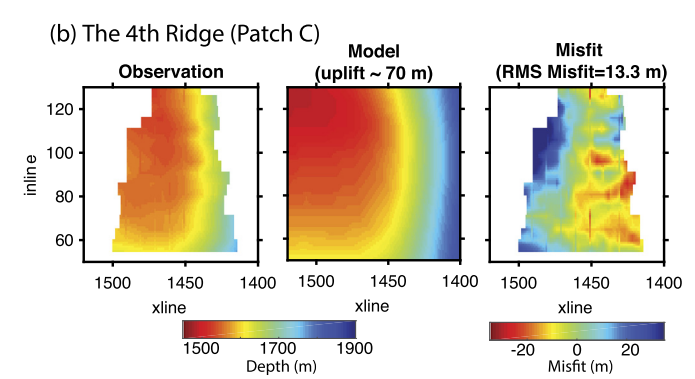
During tectonic uplift, pressure reduction at the seafloor shifts the BGHSZ upwards. As gas hydrate dissociates between the old BGHSZ and the new BGHSZ, two nearly parallel BSRs may co-exist temporarily during this transition (Fig. 9b). In our NZ3D volume, we observe BSR2 that is sub-parallel to BSR1 beneath three thrust ridges (Patches B, C, D) (Fig. 4). We thus consider the hypothesis that these double BSRs are formed by tectonic uplift.

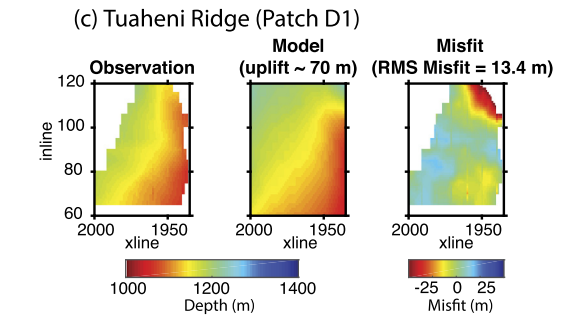
To test this hypothesis, we first estimate the magnitude of uplift needed to produce the observed double BSRs. We model 3D steady-state BGHSZs with paleo-seafloor prior to different amount of uplift and compared the models with the observed BSR2 (Supplementary Information). BSR2 Patches B, C, and D1 can be best modeled with uplift of 45 m, 70 m, and 70 m respectively (Figs. 7, S7). These estimates are similar to the 70 m uplift estimated from 2D seismic images of double BSRs north of our study area (Pecher et al., 2017).

We then estimate the time over which the uplift occurred to determine the uplift rates. For a relic BSR to be seismically imaged, free gas beneath the paleo-BGHSZ is required to produce a negative impedance contrast. We follow the approach of Foucher et al. (2002) and estimated the gas diffusion time to be \sim 14 kyr (Supplementary Information). If hydrate was present above the paleo-BGHSZ, hydrate dissociation can be significantly slowed down with buffering by latent heat during tectonic uplift (Goto et al., 2016), thus helping to preserve BSR2 for longer time. Yet we cannot estimate hydrate dissociation time due to lack of information about the thickness and hydrate saturation of the paleo-hydrate layer. We therefore consider that BSR2 can be seismically recognizable for at least 14 kyr. For 45-70 m of uplift at thrust ridges to happen during this time, the uplift rates are 3-5 mm/yr, higher than the Quaternary uplift estimated from shortening along the east coast of the North Island (<3 mm/yr) (Nicol et al., 2017).

Although the high uplift rate is difficult to achieve with normal subduction scenario, uplift rates can be temporarily substantially







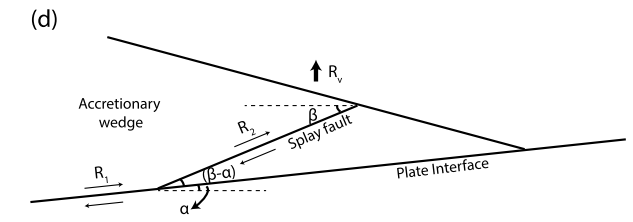


Fig. 7. Analysis of tectonic uplift at thrust ridges the Peak 3B, the 4th Ridge, and the Tuaheni Ridge. (a-c) Depth of observed BSR2, best-fit modeled paleo-BSR prior to tectonic uplift, and the misfit between observation and models for the three ridges (d) Geometry of accretionary wedge with splay fault for calculation of uplift rate. See Table 1 for description of symbols.

larger during localized tectonic events such as seamount subduction, as proposed by Foucher et al. (2002) and Pecher et al. (2017). Along this part of the Hikurangi margin, modeling of magnetic anomaly data suggests the presence of a SW-NE striking, lozenge-

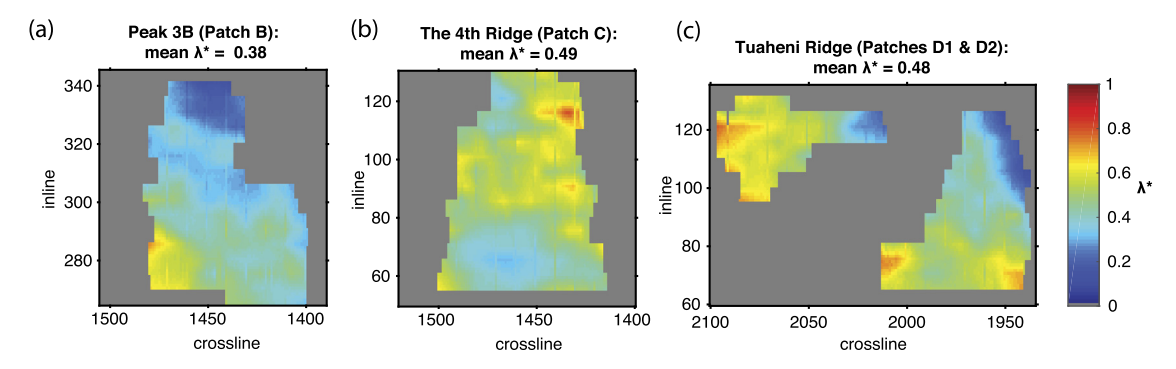


Fig. 8. Modeled overpressure ratio λ^* at the BSR2 depth for (a) Peak 3B (Patch B), (b) The 4th Ridge (Patch C), and (c) the Tuaheni Ridge (Patches D1 & D2).

shaped subducted ridge \sim 40 km long and 15 km wide, with relief up to 2.5 km beneath the eastern part of the Tuaheni Basin (Figs. 1–2) (Barker et al., 2018). A seamount may serve as a barrier for slip propagation along the plate interface and divert slip into the thrust faults in the upper plate (Fig. 7d). During an offshore SSE in September and October 2014, Wallace et al. (2016) observe a gap of large (>10-cm) slip where the subducted ridge is inferred. Apparently, the plate interface updip of the ridge did not slip. Following this SSE, repeating small earthquakes and tremors were detected in the upper plate above the subducted ridge, suggesting slip has been redirected from the plate interface to multiple faults within the upper plate (Shaddox and Schwartz, 2019).

We can estimate uplift rate for this slip scenario by assuming a simple geometry (Fig. 7d). With a subducting plate of dip α and an upper plate thrust fault (splay fault) of dip β , the angle between the plate interface and the splay fault is $(\beta-\alpha)$. We assume that during a short period of time, full convergence rate along the plate interface (R_1) is diverted to a single splay fault. The slip rate along the splay fault is then $R_2 = R_1/\cos(\beta-\alpha)$. The uplift rate associated with the splay fault is $R_v = R_2^* \sin \beta = R_1 / \cos(\beta - \alpha)^* \sin \beta$. At this part of the Hikurangi margin, the plate dip is $\alpha \sim 6^{\circ}$, and the dip of upper plate thrust faults is $\beta \sim 15^{\circ}-30^{\circ}$. With full convergence rate $R_1 = 45$ mm/yr, the uplift rate $R_v = 12-25$ mm/yr. If the convergence is distributed over three upper plate faults beneath Peak 3B, the 4th Ridge, and the Tuaheni Ridge where we observe double BSRs, the average uplift rate would be 4-8 mm/yr for each ridge. These calculated rates are similar to the high uplift rates due to subducted ridges/seamounts observed at southern Central America (3-8.5 mm/yr) (Morell, 2016) and the Solomon Island (8 mm/yr) (Taylor et al., 2005). The uplift rate that we estimated from the double BSRs (3-5 mm/yr) is within the range of the calculated and observed uplift rate related to seamount subduction, therefore we consider double BSRs beneath the thrust ridges can form by tectonic uplift. The 45-70 m uplift that we inferred from double BSRs is likely achieved through multiple uplift events. Only when the quiescence between uplift events is long enough for the hydrate above the old BGHSZ to dissociate and the gas to migrate upwards and accumulate beneath the new BGHSZ, a new BSR can form. That we only observe BSRs at two depths, not at other intermediate depths, may indicate that the guiescence of uplift at these intermediate depths was short compared to the BSR establishment time.

5.2.2. Overpressure caused by fluid migration

Our analysis above has assumed that the BSR2 for Patches B-D is relic BSR. Alternatively, BSR1 and BSR2 may be both modern BSRs formed at different pressure conditions. Fluid overpressure is common at compressional margins. With enhanced pore pressure, the BGHSZ is deeper than with hydrostatic pressure (Fig. 9c). Here we test the hypothesis that the BSR2 for Patches B-D is related to

overpressure caused by fluid migration and investigate its potential link to SSEs along the northern Hikurangi margin.

We first follow the approach of Zander et al. (2017) to calculate overpressure at the BSR2. We assume that BSR1 is at the BGHSZ with hydrostatic pressure to obtain the local thermal gradient and calculate the temperature at BSR2. We then use a methane hydrate stability curve to find the pressure (P) required at this temperature. This pressure lies between hydrostatic (P_{hydro}) and lithostatic pressure (P_{litho}), and we calculate overpressure ratio $\lambda^* = \frac{P - P_{hydro}}{P_{litho} - P_{hydro}}$. We find that if BSR2 is at the BGHSZ with overpressure, the pressures at the BSR2 for Patches B, C, D are higher than P_{hydro} by 1.6 MPa, 2.8 MPa, and 1.7 MPa respectively and their λ^* are \sim 0.4-0.5 (Fig. 8).

For BSR1 and BSR2 to co-exist, we consider the possibility of pressure cycling between hydrostatic pressure, which produces conditions favorable for BSR1, and overpressure $\lambda^* \sim 0.4$ -0.5, which would support BSR2. Such pressure cycling could result from the megathrust earthquake cycle; however, the duration of the cycle may be too long to sustain the overpressure that would support BSR2. SSEs occur every 1-2 years (Wallace et al., 2004), and could also induce pore pressure changes in the overriding plate but on a much shorter time frame, thus allow both pressure conditions to exist for a substantial portion of the slip cycle (Fig. 9c). The SSEs tend to occur in regions with high, near-lithostatic pore fluid pressure along the megathrust (Saffer and Wallace, 2015). Drainage of these highly over-pressured fluids through fracture networks in the overriding plate following SSEs has been inferred from observations of micro-earthquakes and seismic attenuation (Nakajima and Uchida, 2018; Shaddox and Schwartz, 2019; Warren-Smith et al., 2019). We speculate that shortly after an SSE, upward fluid migration increases the pore pressure beneath the thrust ridge and the BGHSZ is at BSR2. Later in the SSE cycle, as the fluid diffuses and pore pressure drops back to hydrostatic, BGHSZ shifts to BSR1 (Fig. 9c). This mechanism requires pressure changes that extend over the 2-3 km wide BSR2 patches. Over-pressured fluid along splay faults could potentially be distributed into the broader region surrounding the BSR2s along secondary faults and highly permeable sand layers (Bense et al., 2013). Although we have no information on whether this is the case, we consider this mechanism as a speculative, yet intriguing link between the double BSRs and SSEs that could be pursued in future studies.

5.2.3. Heat advection caused by fluid migration

The converging geometry of the double BSRs beneath the Peak 3A is curious. We are not aware of any previously reported double BSRs with similar geometry. The polarity of both BSRs is negative, suggesting that free gas is the primary cause of the BSRs (Fig. 5c-f). The waveforms of the double BSRs are more complex than that of BSR1 on the landward side of the ridge, likely reflecting the complex impedance structure within the double BSRs zone as well as interference with reflections from background sedimentary strata.

We suggest that the BSR2 is a younger BSR than the BSR1 and the BGHSZ is moving upwards in this area. Several lines of evidence suggest that this upward shift of BGHSZ is possible and is related to heat advection by fluid migration. (1) Both BSRs beneath the Peak 3A are shallower than the modeled steady state BGHSZ by up to 200 m; yet the BSR1 lies close to the BGHSZ where it is outside of the double BSRs area (Fig. 5a). This distribution is consistent with locally higher heat flow in the double BSRs area. (2) The two BSRs are located within the landward side of a thrust fold that is bounded by a thrust faults to the west (Fig. 5). The \sim 1.4 km thick steeply dipping sediment section that hosts the double BSRs provides ideal conduits for fluid migration. In contrast, landward of the thrust faults where the strata have gentler dips, double BSRs are not observed. (3) The separation of the double BSRs is larger near the apex of the fold, but is smaller away from the apex, consistent with higher fluid flux towards the anticline. Our observations suggest that the double BSRs beneath the Peak 3A are formed by enhanced heat advection associated with fluid migration. Fluid migration due to compaction and mineral dehydration is common at subduction zone margins. When warmer fluid is provided, hydrate dissociates and releases gas that can migrate upwards to form a new BSR at shallower depth. Thus, BSR2 may be a nascent BSR that is forming in response to a new episode of warm fluid migration (Fig. 9d).

6. Causes for widespread double BSRs across the northern Hikurangi margin

Double or multiple BSRs are not commonly observed in marine sediments; however, we imaged multiple patches of double BSRs in our $14 \times 60~\text{km}^2$ survey area. Why are there so many double BSRs along this part of the northern Hikurangi margin?

The abundance of double BSRs may be more apparent from 3D seismic imaging than from 2D profiles. Although multiple patches of double BSRs are observed in our 3D box, they are in general quite limited in spatial extent (a few km across) and cover only 6% of the total area between 650 m and 2750 m water depth. Thus, it is unlikely that sparsely spaced 2D seismic lines will cross double BSRs patches, often leaving them unseen. Furthermore, with 3D data, energy from BSR2 can be better focused through 3D migration and BSR2 can be traced laterally, giving more fidelity in the interpretation of these typically weak reflections. It is possible that double BSRs are widely distributed in other continental margins but are not detected due to lack of 3D seismic data coverage.

Besides the seismic imaging factor, dynamic tectonic processes at the northern Hikurangi margin likely play a major role in the formation of double BSRs. Although the convergence rate at this part of the margin is intermediate among subduction zones, the northern Hikurangi margin may host more vertical tectonic processes due to the many subducting seamounts and ridges. These bathymetric anomalies can impact the accretionary wedge and cause rapid tectonic uplift, and they may also contribute to slope failure and the associated landslide deposit in the forearc basins. These processes all affect the P-T conditions in the shallow sediments, which are key controls for gas hydrate stability.

Furthermore, the abundant fluid of the northern Hikurangi margin may also provide favorable conditions for double BSRs formation. The northern Hikurangi margin has been suggested to be fluid-rich based on its low seismic velocity, high seismic attenuation, and high electrical conductivity (Bassett et al., 2014; Eberhart-Phillips et al., 2017; Heise et al., 2013). A major fluid source is inferred to be subducting sediments (Bell et al., 2010). Frequent SSEs may help maintain high permeability along upper plate faults and thus facilitate episodes of enhanced fluid flow that not only transport deep gas upward, but also modify the thermal

structure and pressure regime at shallow sub-seafloor depth, contributing to the formation of double BSRs.

7. Conclusion

Double BSRs are in general not commonly observed along continental margins. Prior to our study, several causes for double BSRs have been proposed, but they were not well constrained. Now using new 3D seismic data along the northern Hikurangi margin combined with BGHSZ modeling and ocean drilling data, we are able to image multiple patches of double BSRs within a $14 \times 60 \text{ km}^2$ survey area (Figs. 2–5) and provide better constraints and new insights into their formation processes. Specifically, we identify three different formation mechanisms (Fig. 9).

- (1) Rapid sedimentation: Beneath the Tuaheni Basin, the 3D geometry of BSR2 Patch A closely matches that of an unconformity at the base of the basin. Modeling of paleo-seafloor suggests that the BSR2 formed prior to rapid sedimentation in the basin (Fig. 9a).
- (2) *Tectonic uplift:* sub-parallel double BSRs (Patches B, C, D) are imaged beneath three thrust ridges in vicinity of a subducted seamount and their formation can be explained by sustained tectonic uplift at 3-5 mm/yr. This high uplift rate may be achieved when a subducted seamount temporarily diverts all the slip along the plate interface to upper plate thrust faults (Fig. 9b).
- (3) Overpressure/heat advection caused by fluid migration: an alternative formation mechanism for BSR2 Patches B, C, and D involves pore pressure oscillation in the shallow sediments associated with SSEs cycles. The deeper BSR2 is in equilibrium with the high pore pressure ($\lambda^* \sim 0.4$ -0.5) shortly after an SSE when over-pressured fluids at the plate interface migrate upwards through upper plate fracture network and highly dipping strata. The shallower BSR1 is in equilibrium with hydrostatic pressure after the overpressure dissipates later in the SSE cycle (Fig. 9c).

The double BSRs for Patch E converge towards the peak of a thrust ridge and both BSRs are shallower than the modeled steady state BGHSZ. We propose that the shallow BSR may be a nascent BSR forming to adjust to heat advection associated with a new episode of fluid migration (Fig. 9d).

Our study demonstrates that the formation of double BSRs along the northern Hikurangi margin is closely linked to broader-scale subduction processes, not simply local phenomena. Rapid sedimentation in the forearc basins, tectonic uplift caused by seamount subduction, pore pressure fluctuation associated with SSEs, and fluid migration through fault/fracture system in the upper plate all contribute to modulate the P-T conditions in the shallow sediments near the seafloor, providing favorable conditions for double BSRs formation. Our study also shows that double BSRs are manifestation of the dynamics of gas hydrate systems and may be used as indicators for areas with recent sedimentation, tectonic and/or fluid activities at other subduction margins.

CRediT authorship contribution statement

Shuoshuo Han: Conceptualization, Formal analysis, Methodology, Visualization, Writing – original draft. **Nathan L. Bangs:** Funding acquisition, Methodology, Writing – review & editing. **Matthew J. Hornbach:** Software, Writing – review & editing. **Ingo A. Pecher:** Writing – review & editing. **Harold J. Tobin:** Funding acquisition, Writing – review & editing. **Eli A. Silver:** Funding acquisition, Writing – review & editing.

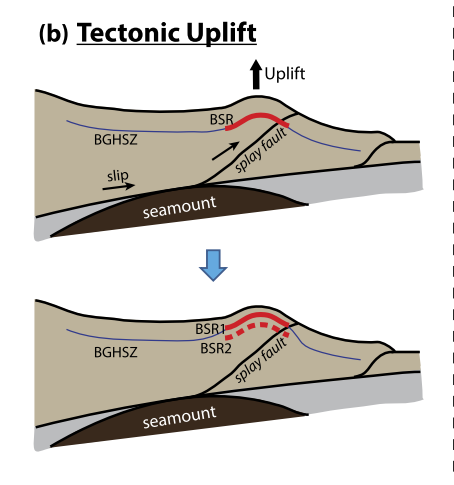
Declaration of competing interest

The authors declare that they have no known competing financial interests or personal relationships that could have appeared to influence the work reported in this paper.

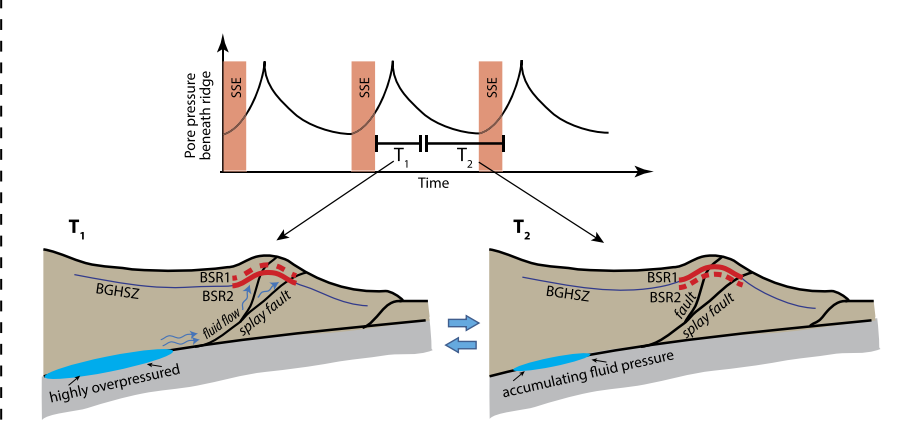
Tuaheni Basin

(a) Rapid sedimentation | State | Sta

Thrust Ridges



(c) Pressure cycling caused by fluid migration associated with SSEs



(d) Heat advection caused by fluid migration

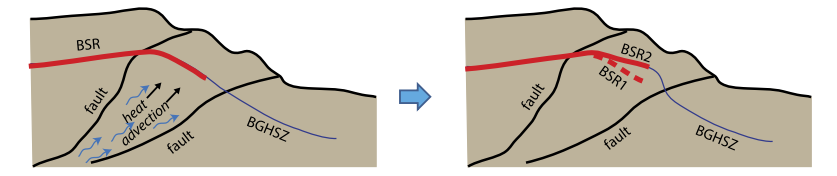


Fig. 9. Summary of double BSRs formation mechanisms along the northern Hikurangi margin determined from NZ3D dataset. (a) Rapid sedimentation; (b) tectonic uplift; (c) pressure cycling caused by fluid migration associated with SSEs; and (d) heat advection caused by fluid migration. Solid red lines of BSR indicate that the BSR is in thermodynamic equilibrium with current P-T conditions. Dashed or dotted red lines of BSR indicate that the BSR is in transient state, i.e. out of thermodynamic equilibrium with current P-T conditions. Thin blue lines indicate BGHSZ.

Acknowledgements

We thank the *R/V M. G. Langseth*'s Captain John Waldrip, crew, and technical staff led by Robert Steinhaus for their efforts, which made possible the success of cruise MGL1801. We thank the science party and staff of International Ocean Discovery Program (IODP) Expeditions 372 and 375 for acquiring the drilling data used in this study. We thank Adrien Arnulf for providing the 2D streamer tomography results, Andrew Gase for providing the locations of seep sites detected from NZ3D water column data, and Kehua You for reviewing an earlier version of the manuscript. We appreciate the constructive reviews by Ann Cook and Tim Minshull that helped to greatly improve this manuscript. Seismic data processing and interpretation was conducted using Echos, GeoDepth, and 3D Canvas software provided by Paradigm Geophysical. This work was supported by the National Science Foundation (grant number 1559298).

Appendix A. Supplementary material

Supplementary material related to this article can be found online at https://doi.org/10.1016/j.epsl.2021.116743.

References

Andreassen, K., Mienert, J., Bryn, P., Singh, S.C., 2000. A double gas-hydrate related bottom simulating reflector at the Norwegian continental margin. Ann. N.Y. Acad. Sci. 912, 126–135.

Bangs, N.L.B., Musgrave, R.J., Tréhu, A.M., 2005. Upward shifts in the southern Hydrate Ridge gas hydrate stability zone following postglacial warming, offshore Oregon. J. Geophys. Res., Solid Earth 110.

Barker, D.H.N., Henrys, S., Caratori Tontini, F., Barnes, P.M., Bassett, D., Todd, E., Wallace, L., 2018. Geophysical constraints on the relationship between seamount subduction, slow slip, and tremor at the North Hikurangi subduction zone, New Zealand. Geophys. Res. Lett. 45, 12,804–812,813.

Bassett, D., Sutherland, R., Henrys, S., 2014. Slow wavespeeds and fluid overpressure in a region of shallow geodetic locking and slow slip, Hikurangi subduction margin, New Zealand. Earth Planet. Sci. Lett. 389, 1–13.

Bell, R., Holden, C., Power, W., Wang, X., Downes, G., 2014. Hikurangi margin tsunami earthquake generated by slow seismic rupture over a subducted seamount. Earth Planet. Sci. Lett. 397, 1–9.

Bell, R., Sutherland, R., Barker, D.H.N., Henrys, S., Bannister, S., Wallace, L., Beavan, J., 2010. Seismic reflection character of the Hikurangi subduction interface, New Zealand, in the region of repeated Gisborne slow slip events. Geophys. J. Int. 180, 34–48.

Bense, V.F., Gleeson, T., Loveless, S.E., Bour, O., Scibek, J., 2013. Fault zone hydrogeology. Earth-Sci. Rev. 127, 171–192.

Bohrmann, G., Torres, M.E., 2006. Gas hydrates in marine sediments, pp. 481-512.

- Chiswell, S.M., Bostock, H.C., Sutton, P.J.H., Williams, M.J.M., 2015. Physical oceanography of the deep seas around New Zealand: a review. N.Z. J. Mar. Freshw. Res. 49, 286–317.
- Collot, J.Y., Lewis, K., Lamarche, G., Lallemand, S., 2001. The giant Ruatoria debris avalanche on the northern Hikurangi margin, New Zealand: result of oblique seamount subduction. J. Geophys. Res., Solid Earth 106, 19271–19297.
- Crutchley, G.J., Gorman, A.R., Pecher, I.A., Toulmin, S., Henrys, S.A., 2011. Geological controls on focused fluid flow through the gas hydrate stability zone on the southern Hikurangi margin of New Zealand, evidenced from multi-channel seismic data. Mar. Pet. Geol. 28, 1915–1931.
- Crutchley, G.J., Mountjoy, J.J., Kellett, R.L., Black, J., Bland, K.J., Coffin, R.B., Field, B.D., Henrys, S.A., Neil, H.L., O'Brien, G., Pecher, I.A., Rose, P.S., Stagpoole, V.M., Strogen, D.P., 2016. Petroleum Prospectivity Screening Report of the Offshore Northern East Coast Basin: GNS Science. GNS Science.
- Davy, B., Hoernle, K., Werner, R., 2008. Hikurangi plateau: crustal structure, rifted formation, and Gondwana subduction history. Geochem. Geophys. Geosyst. 9.
- Eberhart-Phillips, D., Bannister, S., Reyners, M., 2017. Deciphering the 3-D distribution of fluid along the shallow Hikurangi subduction zone using P-and S-wave attenuation. Geophys. J. Int. 211, 1032–1045.
- Foucher, J.-P., Nouzé, H., Henry, P., 2002. Observation and tentative interpretation of a double BSR on the Nankai slope. Mar. Geol. 187, 161–175.
- Goto, S., Matsubayashi, O., Nagakubo, S., 2016. Simulation of gas hydrate dissociation caused by repeated tectonic uplift events. J. Geophys. Res., Solid Earth 121, 3200–3219.
- Greinert, J., Lewis, K.B., Bialas, J., Pecher, I.A., Rowden, A., Bowden, D.A., De Batist, M., Linke, P., 2010. Methane seepage along the Hikurangi margin, New Zealand: overview of studies in 2006 and 2007 and new evidence from visual, bathymetric and hydroacoustic investigations. Mar. Geol. 272, 6–25.
- Haacke, R.R., Westbrook, G.K., Hyndman, R.D., 2007. Gas hydrate, fluid flow and free gas: formation of the bottom-simulating reflector. Earth Planet. Sci. Lett. 261, 407–420
- Heise, W., Caldwell, T.G., Bertrand, E.A., Hill, G.J., Bennie, S.L., Ogawa, Y., 2013. Changes in electrical resistivity track changes in tectonic plate coupling. Geophys. Res. Lett. 40, 5029–5033.
- Holbrook, W.S., Hoskins, H., Wood, W.T., Stephen, R.A., Lizarralde, D., 1996. Methane hydrate and free gas on the Blake Ridge from vertical seismic profiling. Science 273, 1840–1843.
- Hornbach, M.J., Bangs, N.L., Berndt, C., 2012. Detecting hydrate and fluid flow from bottom simulating reflector depth anomalies. Geology 40, 227–230.
- Huhn, K., 2016. SlamZ: slide activity on the Hikurangi margin, New Zealand. Cruise Report SO247.
- Milkov, A.V., Sassen, R., 2000. Thickness of the gas hydrate stability zone, Gulf of Mexico continental slope. Mar. Pet. Geol. 17, 981–991.
- Morell, K.D., 2016. Seamount, ridge, and transform subduction in southern Central America. Tectonics 35, 357–385.
- Mountjoy, J.J., McKean, J., Barnes, P.M., Pettinga, J.R., 2009. Terrestrial-style slow-moving earthflow kinematics in a submarine landslide complex. Mar. Geol. 267, 114–127.
- Nakajima, J., Uchida, N., 2018. Repeated drainage from megathrusts during episodic slow slip. Nat. Geosci. 11, 351–356.
- Nicol, A., Seebeck, H., Wallace, L., 2017. Quaternary tectonics of New Zealand, pp. 1–34.
- Paganoni, M., Cartwright, J.A., Foschi, M., Shipp, R.C., Van Rensbergen, P., 2016. Structure II gas hydrates found below the bottom-simulating reflector. Geophys. Res. Lett. 43, 5696–5706.

- Pecher, I.A., Barnes, P.M., LeVay, L.J., Scientists, t.E., 2019. Creeping gas hydrate slides. In: Proceedings of the International Ocean Discovery Program, 372A. College Station, TX (International Ocean Discovery Program).
- Pecher, I.A., Villinger, H., Kaul, N., Crutchley, G.J., Mountjoy, J.J., Huhn, K., Kukowski, N., Henrys, S.A., Rose, P.S., Coffin, R.B., 2017. A fluid pulse on the Hikurangi subduction margin: evidence from a heat flux transect across the upper limit of gas hydrate stability. Geophys. Res. Lett. 44, 12,385–312,395.
- Pedley, K.L., Barnes, P.M., Pettinga, J.R., Lewis, K.B., 2010. Seafloor structural geomorphic evolution of the accretionary frontal wedge in response to seamount subduction, poverty indentation, New Zealand. Mar. Geol. 270, 119–138.
- Popescu, I., De Batist, M., Lericolais, G., Nouzé, H., Poort, J., Panin, N., Versteeg, W., Gillet, H., 2006. Multiple bottom-simulating reflections in the Black Sea: potential proxies of past climate conditions. Mar. Geol. 227, 163–176.
- Ruppel, C.D., Kessler, J.D., 2017. The interaction of climate change and methane hydrates. Rev. Geophys. 55, 126–168.
- Saffer, D.M., Wallace, L.M., 2015. The frictional, hydrologic, metamorphic and thermal habitat of shallow slow earthquakes. Nat. Geosci. 8, 594–600.
- Schneider, W.A., Backus, M.M., 1968. Dynamic correlation analysis. Geophysics 33, 105–126.
- Screaton, E.J., Torres, M.E., Dugan, B., Heeschen, K.U., Mountjoy, J.J., Ayres, C., Rose, P.S., Pecher, I.A., Barnes, P.M., LeVay, L.J., 2019. Sedimentation controls on methane-hydrate dynamics across glacial/interglacial stages: an example from International Ocean Discovery Program Site U1517, Hikurangi margin. Geochem. Geophys. Geosyst. 20, 4906–4921.
- Shaddox, H.R., Schwartz, S.Y., 2019. Subducted seamount diverts shallow slow slip to the forearc of the northern Hikurangi subduction zone, New Zealand. Geology 47, 415–418.

Sloan, E.D., Koh, C.A., 2007. Clathrate hydrates of natural gases.

- Taylor, F.W., Mann, P., Bevis, M.G., Edwards, R.L., Cheng, H., Cutler, K.B., Gray, S.C., Burr, G.S., Beck, J.W., Phillips, D.A., 2005. Rapid forearc uplift and subsidence caused by impinging bathymetric features: examples from the New Hebrides and Solomon arcs. Tectonics 24.
- Wallace, L.M., 2020. Slow slip events in New Zealand. Annu. Rev. Earth Planet. Sci. 48.
- Wallace, L.M., Beavan, J., McCaffrey, R., Darby, D., 2004. Subduction zone coupling and tectonic block rotations in the North Island, New Zealand. J. Geophys. Res., Solid Earth 109.
- Wallace, L.M., Saffer, D.M., Barnes, P.M., Pecher, I.A., Petronotis, K.E., LeVay, L.J., Scientists, t.E., 2019. Hikurangi subduction margin coring, logging, and observatories. In: Proceedings of the International Ocean Discovery Program, 372B/375. College Station, TX (International Ocean Discovery Program).
- Wallace, L.M., Webb, S.C., Ito, Y., Mochizuki, K., Hino, R., Henrys, S., Schwartz, S.Y., Sheehan, A.F., 2016. Slow slip near the trench at the Hikurangi subduction zone, New Zealand. Science 352, 701–704.
- Warren-Smith, E., Fry, B., Wallace, L., Chon, E., Henrys, S., Sheehan, A., Mochizuki, K., Schwartz, S., Webb, S., Lebedev, S., 2019. Episodic stress and fluid pressure cycling in subducting oceanic crust during slow slip. Nat. Geosci. 12, 475–481.
- Zander, T., Haeckel, M., Berndt, C., Chi, W.-C., Klaucke, I., Bialas, J., Klaeschen, D., Koch, S., Atgı, n O., 2017. On the origin of multiple BSRs in the Danube deepsea fan, Black Sea. Earth Planet. Sci. Lett. 462, 15–25.